# Establishing Water-Soluble Layered WS$_2$ Nanosheet as a Platform for Biosensing

Yunxia Yuan, Runqing Li, and Zhihong Liu*

Key Laboratory of Analytical Chemistry for Biology and Medicine (Ministry of Education), College of Chemistry and Molecular Sciences, Wuhan University, Wuhan, Hubei 430072, China

S *Supporting Information*

ABSTRACT: Layered WS$_2$ nanosheet is a kind of two-dimensional (2D) covalent-network solid material with remarkable structural and electronic properties that has attracted increasing interest in recent years. In this work, we propose a one-step sonication-assisted exfoliation method to prepare water-soluble WS$_2$ nanosheet and demonstrate its application as a biosensing platform. The synthesis route is simple and straightforward. We reveal that single-strand DNA (ssDNA) chains can readily be adsorbed on the nanosheet, leading to complete and fast quenching of a fluorescent dye tagged to the DNA chain. The adsorbed ssDNA is detachable from the nanosheet upon the interaction with other biomolecules, resulting in the restoration of the fluorescence. The 2D WS$_2$ nanosheet thus acts as an efficient platform for assembling of bioprobes. Because of the extraordinarily high quenching efficiency, which is the synergic result of both excited-state energy transfer and static quenching, the WS$_2$ platform affords minimal background and high sensitivity. Our attempt will extend the application of this material to biosensing and probing areas.
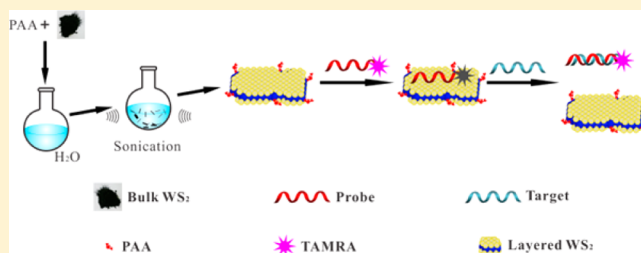
In recent years, layered two-dimensional (2D) transition metal dichalcogenides (TMDCs) with single or few atomic layers, recognized as planar covalent-network solids, have attracted growing attention owing to their special structures with high specific surface area and remarkable electronic properties catering for intriguing applications in optoelectronics and energy harvesting.[1−5] As one of the newly emerging 2D TMDCs, layered tungsten disulfide (WS$_2$) that consists of S−W−S sandwiches in a trigonal prismatic coordination has shown promising prospect in the field of catalyst, field-effect transistor, lithium ion batteries, and so on.[6−9] In the past several years, considerable efforts have been made to the synthesis of WS$_2$ nanosheet by different routes, which mainly include liquid-phase exfoliation and Li$^+$ intercalation.[10−14] Bulk WS$_2$ is a layered compound with strong W−S bonding in-plane and weak van der Waals interaction out-of-plane, allowing exfoliation into individual ultrathin layers. Unfortunately, layered WS$_2$ nanosheet obtained from liquid-phase exfoliation in organic solvents exhibits poor solubility in water, which limits its range of use, for instance, in biological applications. Although water-soluble WS$_2$ nanosheet can be prepared by the Li$^+$ ion intercalation method, this synthesis route is extremely sensitive to environmental conditions; besides, it tends to cause the structural deformation which considerably alters the electronic properties. Partly due to the lack of effective ways to acquire water-solubility,[15] the biological application of 2D WS$_2$, unlike other 2D covalent crystals such as graphene,[16,17] MnO$_2$,[18,19] and MoS$_2$,[20] is rarely reported. Layered WS$_2$ nanosheet and its composites were recently applied in electrochemical biosensing,[21,22] and most recently, commercial WS$_2$ nanosheet dispersed in ethanol solution was used in the detection of MicroRNA.[23] Nevertheless, it is still significant to acquire water-soluble layered WS$_2$ nanosheet and explore its application as a universal biosensing platform.

We herein proposed a one-step and facile route to fabricate water-soluble WS$_2$ nanosheet and demonstrated its usage in biosensing. By utilizing the strong coordination effect of carboxyl groups with tungsten atoms, layered WS$_2$ nanosheet functionalized with poly(acrylic acid) (PAA) was obtained through sonication-assisted exfoliation of bulk WS$_2$. Our results revealed that the large lateral dimensions and high surface areas of layered WS$_2$ enabled easy assembly of biological probes which led to efficient quenching of the tagged fluorophores, and the fluorophore-labeled probes could readily be desorbed from the surface of WS$_2$ nanosheet upon a target-induced conformation change. On the basis of these findings, highly sensitive and specific sensing of nucleic acid and protein was achieved, which discovered the extended application of layered WS$_2$ nanosheet in biological sensing areas.

■ EXPERIMENTAL SECTION

Apparatus. The size and morphologies of WS$_2$ nanosheet were characterized by a JEM-2010 transmission electron microscope (TEM) with an acceleration voltage of 100 kV (Hitachi H-7000FA, Japan) and field-emission scanning

electron microscopy (FE-SEM) (Hitachi SU8010, Japan). Atomic force microscope (AFM) images of layered WS$_2$ were acquired with a tapping mode and a 1024 × 1024 pixel resolution (Benyuan-CSPM5500, China) and analyzed with a CSPM Console software (Benyuan-CSPM5500, China). The EDX spectra were recorded with a scanning electron microscopy (SEM) (FEI Quanta 200). FI-IR spectra were measured on a Magan-IR spectrometer 500 (Nicolet, Madision, WI) with the KBr pellet technique. UV−vis absorption spectra data were recorded with a UV-2550 spectrophotometer (Shimadzu, Tokyo, Japan). Fluorescence spectra were collected with a RF-5301PC fluorescence spectrophotometer (Shimadzu, Tokyo, Japan). Time-resolved fluorescence decay experiments were performed on a FELIX32 system (Photon Technology International).

Materials. Bulk tungsten sulfide (WS$_2$) was commercially available from Aladdin (Shanghai, China). Polyacrylic acid (PAA, with an average molecular weight of 1800) was purchased from Sigma-Aldrich. Carcinoembryonic antigen (CEA) was bought from Boster Co., Ltd. (Wuhan, China). The rest of the chemical reagents were purchased from Sinopharm Chemical Reagent Co., Ltd. (Shanghai, China). All aqueous solutions were prepared using Mill-Q water (Millipore, 18.2 MΩ resistivity). All DNA sequences were synthesized and purified by Sangon Biotech Co., Ltd. (Shanghai, China), and their base sequences were as follows: (1) the TAMRA dye-labeled ssDNA probe P1: 5′-TAMRA-AGTCAGTGTGGA-AAATCTCTAGC-3′; (2) the complementary target DNA T1: 5′-GCTAGAGATTTTCCACACTGACT-3′; (3) the single-base mismatched ssDNA (SBM se-quence): 5′-GCTAGAGA-TTGTCCACACTGACT-3′; (4) the noncomplementary ssDNA (NC sequence): 5′-ATAGTGATGCAAGTGGTAAC-GGC-3′; (5) the TAMRA dye-labeled CEA aptamer (probe P2): 5′-TAMRA-ATACCAGCTTATTCAATT-3′.

Synthesis of Layered WS$_2$ Nanosheet. The PAA modified WS$_2$ nanosheet was synthesized from bulk WS$_2$ by sonication-assisted liquid exfoliation in water. In a typical procedure, WS$_2$ powder (150 mg) and PAA (50 mg) were added to a 50 mL flask containing 20 mL of ultrapure water as the solvent and the mixture was sonicated for 6 h. Then, the dark green dispersion was centrifuged at 3000 rpm for 10 min to remove large-size masses. The supernatant was collected and further washed with water by centrifugation at 10 000 rpm for 5 min. The as-obtained black precipitate was dispersed in water for further characterizations and applications, and the layered WS$_2$ nanosheet without PAA modification was prepared via a similar process without PAA using 1-methyl-2-pyrrolidinone (NMP) as the solvent.

Sensing of the Target DNA. To an aqueous solution containing 50 nM probe P1, different amounts of target DNA T1 (ranging from 0.1−150 nM) were added and incubated at 37 °C for 60 min. After the addition of WS$_2$ nanosheet (60 μg/mL), the mixtures were allowed to react for 30 min at room temperature prior to the fluorescence measurement. All the solutions were prepared in 10 mM Tris-HCl buffer (pH 7.4, containing 100 mM NaCl).

Sensing of Protein CEA. 50 nM probe P2 was incubated with different concentrations of CEA at 37 °C for 60 min prior to the addition of WS$_2$ nanosheet (80 μg/mL). The final CEA concentration in samples ranged from 1 to 200 ng/mL. After incubating the mixtures for 30 min at room temperature, a fluorescence measurement was performed. All the solutions

were prepared in 10 mM Tris-HCl buffer (pH 7.4, containing 100 mM NaCl).

■ RESULTS AND DISCUSSION

Synthesis and Characterization of Water-Soluble WS$_2$ Nanosheet. PAA modified WS$_2$ nanosheet was synthesized with a one-step procedure, by simply exfoliating bulk WS$_2$ under sonication in the presence of PAA molecules (Scheme S1, Supporting Information) in water, followed by removal of large-size masses and unbound PAA with centrifugation. With the assistance of continuous sonication for a certain period of time, the bulk solid material was split to lamellar structures with the lateral size ranging from tens to hundreds of nanometer, as shown with the image of field-emission scanning electron microscopy (FE-SEM) (Figure 1A). The transmission electron
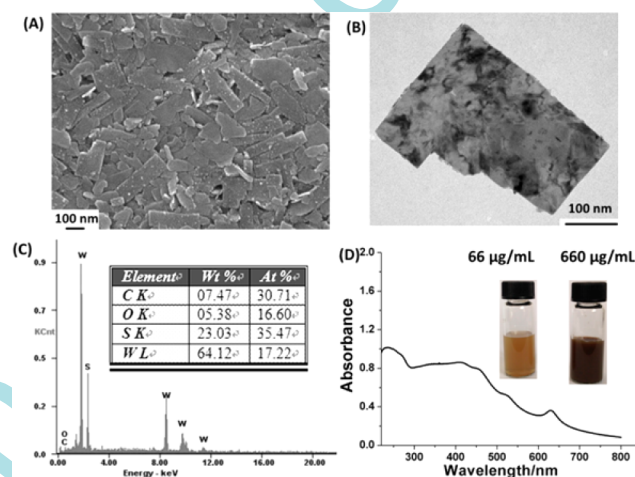

Figure 1. (A) FE-SEM image of the as-synthesized layered WS$_2$ nanosheet; scale bar: 100 nm. (B) TEM image of the as-synthesized layered WS$_2$ nanosheet; scale bar: 100 nm. (C) EDS spectrum of the layered WS$_2$ nanosheet; the inset table shows the calculated weight and molar compositions. (D) UV−vis spectrum of the as-synthesized layered WS$_2$ nanosheet. Inset: the photograph of the product in aqueous solution after being stored for 10 days.

microscopy (TEM) image of a representative dispersed product further revealed that the morphology was a two-dimensional thin-layer nanosheet (Figure 1B). The thickness of the as-obtained WS$_2$ sheet measured with atom force microscopy (AFM) was around 1.0 nm (Figure S1A, Supporting Information), suggesting its single-layer structure. The elemental composition of the product was identified with energy-dispersive spectroscopy (EDS), which showed intense peaks of W and S (Figure 1C). The molar ratio of W/S was calculated as 17.22:35.47 (which is approximately 1:2) from the peak intensities (the inserted table in Figure 1C), verifying the desired stoichiometry of the products. Besides, the EDS data also indicted the existence of elements C and O, which can be assigned to PAA molecules that bound to WS$_2$ through the coordination of PAA carboxyl with the unsaturated W atom at the edge of WS$_2$ nanosheet.[24] A further evidence of the existence of PAA molecules was provided by FT-IR measurement. The FT-IR spectra (Figure S2A, Supporting Information) showed the characteristic absorption peaks of −OH stretching (3550−3000 cm^{-1}), C=O stretching vibration (1652 cm^{-1}), C−O stretching (1188 cm^{-1}), and symmetric COO− stretching (1396 cm^{-1}), which confirmed the successful

3611

dx.doi.org/10.1021/ac5002096 | *Anal. Chem.* 2014, 86, 3610−3615

functionalization of the product with PAA during the process of sonication. The thermogravimetric (TG) curve of layered WS_2 nanosheet (Figure S2B, Supporting Information) allowed the estimation of the mole fraction ratio between WS_2 and PAA to be about 60:1.

This fabrication method is relatively simple and straightforward and can be scaled up to give large quantities of products. Note also that we used an ordinary ultrasonic cleaner with 100 W power and 40 kHz frequency for the preparation, which is cost-effective and can be achievable in most laboratories. Because of the surface modification with PAA molecules, the water suspension of the nanosheet was highly stable and showed no precipitation after being stored for weeks under ambient conditions, which is also verified by the fact that the layered WS_2 nanosheet was negatively charged with a zeta potential of <-30 mV in aqueous solution in the pH range of 6.6−8.0 (Figure S3, Supporting Information). In addition, the carboxyl groups on the surface also can provide potential reaction sites for conjugation with other substances for later biological applications. The light absorption of the PAA modified WS_2 nanosheet was detected and shown in Figure 1D. A typical absorption peak of WS_2 nanosheet at 627 nm[14] was observed, which was linearly related to the concentration of WS_2 nanosheet (Figure S4, Supporting Information). The extinction coefficient was estimated to be 7885 mL/mg/m, slightly larger than the reported value.[14] It is seen that the light absorption covers a wide range from UV to visible region, which suggests that the material can be a versatile energy harvester (acceptor) for diverse luminophors.

Principle of the Sensing Platform Based on WS_2 Nanosheet. According to an earlier study which showed that long-chain hydrocarbons could be adhered on the surface of WS_2 solids,[25] we anticipated that the 2D WS_2 nanosheet could act as a nanoplatform to adsorb biomolecules like oligonucleotides and peptides, which can be subsequently employed as biological probes. In addition, in consideration of the established energy harvesting properties, we also expected the WS_2 nanosheet to quench luminescence of fluorophores via energy transfer processes, so that optical biosensing systems with the nanosheet as an energy acceptor (quencher) could be built. To investigate the applicability of the layered WS_2 nanosheet in biosensing, we designed homogeneous fluorescence assays based on the fluorescence quenching-restoration principle using WS_2 nanosheet as the dark quencher, as shown in Scheme 1. Single-strand DNA (ssDNA) chains were used as the probes, which were prelabeled with a fluorescent dye, tetramethylrhodamine (TAMRA). Similar to the situations of those previously reported 2D covalent-network crystals, we speculated that the fluorescence of the dye would be quenched by WS_2 due to the physisorption (mainly van der Waals interaction[20]) of the probes on the nanosheet which takes the dye and the WS_2 nanosheet into close proximity or molecular contact. Subsequently, restoration of the fluorescence was expected upon the introduction of sensing targets, which react with the DNA probes and alter their molecular conformation leading to weakened physisorption because the nucleobases are shielded by the phosphate backbone in such situations. In order to check which kind of biochemical reaction is able to adequately change the binding state of the ssDNA probe on WS_2 nanosheet and to examine the universality of the proposed fluorescence sensing protocol as well, we constructed two biosensors utilizing two different target recognition models, i.e.,

Scheme 1. Schematic Illustration of Fluorescence Sensing of Nucleic Acid and Protein with Layered WS_2 Nanosheet as the Quencher[a]
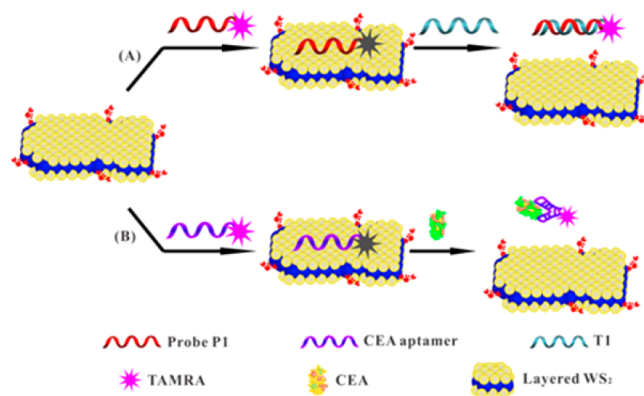
[a]Not to scale.

a nucleic acid hybridization model and a protein−aptamer reaction model, respectively (Scheme 1A, 1B).

Hybridization Assay of Target DNA with the WS_2 Nanosheet-Based Biosensor. To realize the idea of layered WS_2-based biosensing, we first utilized an ssDNA chain (named as P1) targeting a DNA sequence from the human immunodeficiency virus type 1 (HIV-1) U5 long terminal repeat sequence as a model probe, which was prelabeled with a TAMRA dye. First of all, we accessed the feasibility of adjusting the binding state of the ssDNA probe on the WS_2 nanosheet via a study of fluorescence anisotropy (FA). It is known that the FA of a fluorophore reflects the ability of the molecule to rotate in its microenvironment, and fluorescence anisotropy measurements are commonly used to probe molecular interactions.[26] We investigated the adsorption of the probe P1 on WS_2 nanosheet before and after the addition of target DNA by measuring the fluorescence anisotropy of the tagged dye. As shown in Figure S5, Supporting Information, the FA value of TAMRA on the free probe P1 in an aqueous buffer solution was 0.333, and it increased to 0.593 after adding WS_2 nanosheet to the solution, indicating that the dye-labeled probe DNA was assembled onto the surface of WS_2 nanosheet which restricted the rotation of the dye. Thereafter, upon the addition of the target DNA (T1) that hybridized with the probe, the FA value was reduced back to 0.368, which was close to that of the free ssDNA probe and suggested that the hybridization of P1 with the complementary target DNA effectively decreased the adsorption of P1 on WS_2 nanosheet. These results primarily confirmed our above speculations. Further evidence of the adsorption was also found from AFM measurements of WS_2 nanosheet in the presence of the probe. The AFM analysis revealed that the height of the WS_2 nanosheet increased from 1 nm to ca. 1.6 nm after the addition of probe P1 (Figure S1B, Supporting Information), which can be another indicator of the adsorbing state.

Figure 2A shows the quenching of TAMRA fluorescence by WS_2 nanosheet, which was dependent on the concentration of the quencher. In the presence of a small amount (60 μg/mL) of WS_2 nanosheet, the emission of the dye was quenched to baseline level, indicating a high efficiency of layered WS_2 nanosheet as a dark quencher. In addition, the quenching kinetics of the system (Figure 2B) suggested that the interaction of the ssDNA probe with WS_2 nanosheet was a
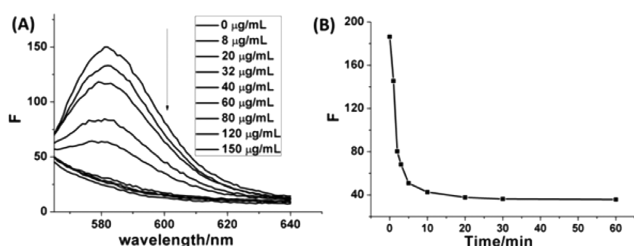
Figure 2. (A) Fluorescence quenching of probe P1 (50 nM) in the presence of an increasing amount of WS$_2$ nanosheet (0, 8, 20, 32, 40, 60, 80, 120, and 150 μg/mL). (B) Fluorescence quenching of probe P1 (50 nM) by WS$_2$ (60 μg/mL) as a function of time. Experiments were performed in Tris-HCl buffer (10 mM, pH 7.4, containing 100 mM NaCl). Excitation wavelength: 530 nm; emission wavelength: 583 nm.

quite fast process that reached to equilibrium in about 20 min, which was a competitive performance among the 2D covalent-network solids for biosensing. As compared to graphene, the most widely used 2D nanoplatform as luminescence quencher, WS$_2$ nanosheet exhibits a notable merit that the quenching efficiency is more robust because of the easier acquisition of water solubility. It is known that the conjugated network consisting of sp^2-hybridized carbon atoms is essential for the quenching ability of graphene and that the graphitic material needs to be partially oxidized to acquire water solubility. The surface oxidation will change the carbon hybridization from sp^2 to sp^3 which impairs the quenching ability. Therefore, the extent of surface oxidation of graphene always needs special care because of its opposite effects on the quenching efficiency and solubility.[17,27]

The sensor was then applied to the detection of the target DNA with a homogeneous assay protocol. After introducing an increasing amount of the target sequence T1 to the sensing system, the emission of TAMRA was gradually recovered as expected (Figure 3A), which was a result of the separation of
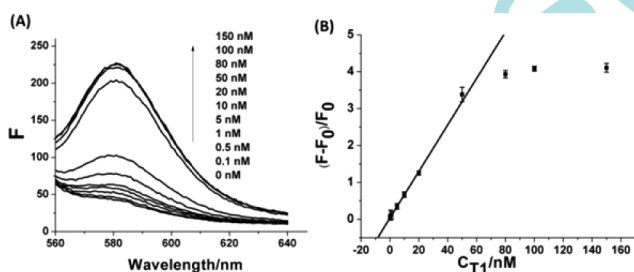

Figure 3. (A) Fluorescence emission of the sensor in the presence of different amounts of target T1 (0, 0.1, 0.5, 1, 5, 10, 20, 50, 80, 100, and 150 nM). (B) The dependence of the relative fluorescence intensity on T1 concentration and the linear calibration within the range of 0.1−50 nM. Data were presented as average ± sd from three independent measurements. Experiments were performed in Tris-HCl buffer (10 mM, pH 7.4, containing 100 mM NaCl). Excitation wavelength: 530 nm; emission wavelength: 583 nm.

the dye from WS$_2$ nanosheet induced by the probe-to-target hybridization. The plot of the relative fluorescence intensity ($F − F_0)/F_0$ (where F_0 and F represent the fluorescence intensity at 583 nm in the absence and presence of T1, respectively) versus the concentration of T1 showed a linear dependence within the range from 0.1 to 50 nM (Figure 3B), which can be adopted for quantification of the target DNA. Owing to the

above-mentioned high efficiency of fluorescence quenching which contributed to lowered background, the WS$_2$ nanosheet-based DNA sensor exhibited favorable sensitivity with a limit of detection (LOD) of 60 pM ($3\sigma/k$, $n = 11$, where σ is the standard deviation for the blank solution and k is the slope of the linear calibration curve), which is lower than the reported GO and MoS$_2$-based DNA sensing.[20,28,29]

We further looked into the specificity of the sensor by comparing the fluorescence responses toward the target-DNA (T1), a single-base mismatched (SBM) sequence, and a noncomplementary (NC) sequence at the same concentration. As shown in Figure S6, Supporting Information, the fluorescence recovery ($(F − F_0)/F_0$) with 50 nM SBM DNA was only 64% of that obtained with the target T1, and the addition of 50 nM NC DNA caused nearly negligible alteration of the fluorescence intensity. The results demonstrated pronounced specificity of the sensor, and the ability to discriminate single-base mismatch may hold great promise for single-nucleotide polymorphism detection applications.

Sensing of Protein CEA with the WS$_2$ Nanosheet-Based Biosensor. Thus far, we have revealed the applicability of the water-soluble layered WS$_2$ nanosheet in biomolecule sensing, by utilizing the different affinities of ssDNA and dsDNA on the nanosheet. To examine whether other kinds of interaction between biomolecules, such as the protein−aptamer reaction, can also be employed to control the binding state of biological probes on WS$_2$ nanosheet, we constructed another sensor for protein assay with an aptamer as the probe. Aptamers are special functional nucleotide sequences that have been selected toward a large pool of targets with high selectivity and affinity.[30,31] We chose the protein carcinoembryonic antigen (CEA), a tumor marker, as the proof-of-principle target, and accordingly, the CEA aptamer containing 18 bases (named as P2) was used for labeling with the dye TAMRA. Before we moved on to the protein sensing, we also checked the binding of the aptamer probe on WS$_2$ nanosheet first. The FA value of the dye increased from 0.257 (on the free probe P2) to 0.622 (with the addition of WS$_2$ nanosheet) and then fell back to 0.293 (after adding the protein CEA) (Figure S7, Supporting Information). The evolution of FA value of the dye clearly indicated that the aptamer probe adsorbed on WS$_2$ nanosheet was desorbed from the nanosheet upon reacting with the protein.

Similar to the above case of probe P1, the emission of TAMRA tagged to P2 was also thoroughly quenched by WS$_2$ nanosheet (to the baseline level, Figure 4A). The time course of the fluorescence intensity (Figure 4B) exhibited a complete quenching within just 10 min, which was shorter than that of probe P1 containing 23 bases. This result suggested that the quenching kinetics was dependent on the length of the ssDNA probe, that is, shorter sequence leads to faster kinetics, which was also observed in graphene-based DNA probes.[28] In the presence of CEA that formed an inosculating complex with the aptamer, the fluorescence intensity of TAMRA was recovered (Figure 4C), and the relative fluorescence intensity also exhibited a linear relationship with the concentration of CEA in the range of 1.0−80 ng/mL (Figure 4D).

Possible Mechanism of Fluorescence Quenching by WS$_2$ Nanosheet. The possible mechanism underlying the fluorescence quenching of the luminophors by WS$_2$ nanosheet was inspected by taking the probe P2 as an example. In light of the well-defined energy harvesting property of WS$_2$, we supposed that an energy transfer process from the excited
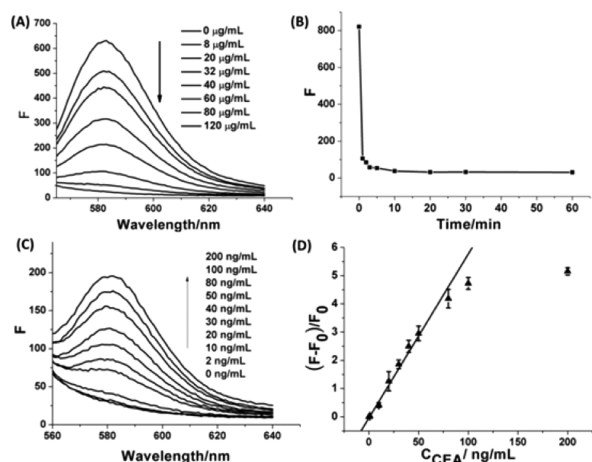
Figure 4. (A) Fluorescence quenching of probe P2 (50 nM) in the presence of WS_2 nanosheet with a series of concentrations (0, 8, 20, 32, 40, 60, 80, and 120 μg/mL). (B) Fluorescence quenching of probe P2 (50 nM) by WS_2 nanosheet (80 μg/mL) as a function of time. (C) Fluorescence emission of the sensor in the presence of different amounts of CEA (0, 1, 10, 20, 30, 40, 50, 80, 100, and 200 ng/mL). (D) The dependence of the relative fluorescence intensity on CEA concentration and the linear calibration within the range of 1−80 ng/mL. Data were presented as average ± sd from three independent measurements. Experiments were performed in Tris-HCl buffer (10 mM, pH 7.4, containing 100 mM NaCl). Excitation wavelength: 530 nm; emission wavelength: 583 nm.

dye to the quencher would have occurred. To prove this, we measured the lifetime of the dye in the presence of different amounts of WS_2. The time-resolved fluorescence decay curves of TAMRA labeled on probe P2 are shown in Figure 5A, which
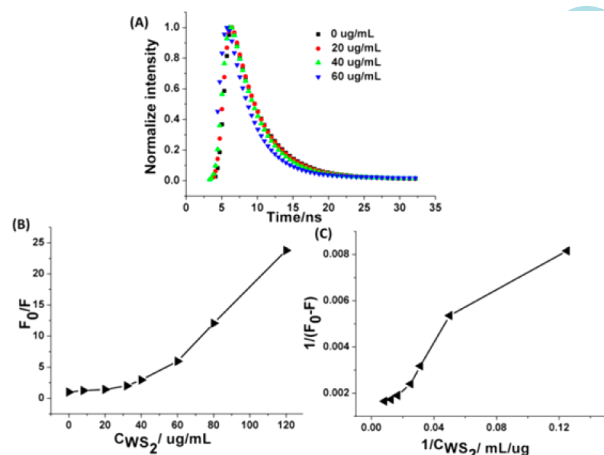

Figure 5. (A) Time-resolved fluorescence decay curves of TAMRA labeled to probe P2 (50 nM) in the presence of different amounts of WS_2 nanosheet. (B) The Stern−Volmer plot of the quenching system (with 50 nM P2). (C) The Lineweaver−Burk plot of the quenching system (with 50 nM P2). Experiments were performed in Tris-HCl buffer (10 mM, pH 7.4, containing 100 mM NaCl).

revealed that the fluorescence lifetime did decrease along with the increase of WS_2 amount, indicating the occurrence of dynamic quenching. However, from the lifetime values calculated according to the curves (Table S1, Supporting Information), we found that the reduction in fluorescence lifetime was not equal to the reduction in fluorescence intensity at all the three WS_2 concentrations investigated. It implied that

the fluorescence quenching was not the result of a single mechanism. As further evidence shows in Figure 5B,C, the fluorescence quenching did not properly fit to either the Stern−Volmer equation or the Lineweaver−Burk equation. The Stern−Volmer plot exhibited an upward curvature concaving toward the *y*-axis, which is the characteristic feature of the combination of dynamic and static quenching.[26] Although the contribution of each part to the observed quenching still needs further examination, the coexistence of both dynamic and static quenching might have explained the highly efficient quenching of the dye by the layered WS_2 nanosheet, which is in favor of quenching-and-recovery-based sensing.

■ CONCLUSION

In summary, we have developed a one-step procedure to synthesize layered WS_2 nanosheet with high dispersibility in water. The 2D nanosheet acts as a platform for easy assembly of biological probes and affords high efficiency to quench the emission of luminophors on or near the surface. Besides, the binding of the bioprobes on WS_2 nanosheet is a reversible process that can be controlled by interactions of the probes with other biomolecules, which enables a facile mix-and-detect assay strategy for biosensing. The merits of this work include (1) the synthesis route is very simple and can be scaled up or extended to other layered covalent-network solids, (2) the layered WS_2 nanosheet provides low background and high sensitivity in fluorescence assays, and it also holds great versatility to develop biosensors for a wide spectrum of targets, and (3) our efforts may open the way to the preparation and biological application of other water-soluble 2D covalent crystals.

■ ASSOCIATED CONTENT

Ⓢ Supporting Information
Characterization, fluorescence anisotropy of P1 and P2 after the interaction with WS_2 nanosheet and the target, and specificity of probe P1. This material is available free of charge via the Internet at http://pubs.acs.org.

■ AUTHOR INFORMATION

Corresponding Author
*E-mail: zhhliu@whu.edu.cn. Phone: 86-27-87217886. Fax: 86-27-68754067.

Notes
The authors declare no competing financial interests.

■ ACKNOWLEDGMENTS

■ REFERENCES

(1) Wang, Q. H.; Kalantar-Zadeh, K.; Kis, A.; Coleman, J. N.; Strano, M. S. *Nat. Nanotechnol.* **2012**, *7*, 699−712.
(2) Xu, M.; Liang, T.; Shi, M.; Chen, H. *Chem. Rev.* **2013**, *113*, 3766−3798.
(3) Huang, X.; Zeng, Z.; Zhang, H. *Chem. Soc. Rev.* **2013**, *42*, 1934−1946.
(4) Butler, S. Z.; Hollen, S. M.; Cao, L.; Cui, Y.; Gupta, J. A.; Gutiérrez, H. R.; Heinz, T. F.; Hong, S. S.; Huang, J.; Ismach, A. F.; Halperin, E. J.; Kuno, M.; Plashnitsa, V. V.; Robinson, R. D.; Ruoff, R.

S.; Salahuddin, S.; Shan, J.; Shi, L.; Spencer, M. G.; Terrones, M.; Windl, W.; Goldberger, J. E. *ACS Nano* **2013**, *7*, 2898−2926.

(5) Chhowalla, M.; Shin, H. S.; Eda, G.; Li, L. J.; Loh, K. P.; Zhang, H. *Nat. Chem.* **2013**, *5*, 263−275.

(6) Voiry, D.; Yamaguchi, H.; Li, J.; Silva, R.; Alves, D. C. B.; Fujita, T.; Chen, M.; Asefa, T.; Shenoy, V. B.; Eda, G.; Chhowalla, M. *Nat. Mater.* **2013**, *12*, 850−855.

(7) Georgiou, T.; Jalil, R.; Belle, B. D.; Britnell, L.; Gorbachev, R. V.; Morozov, S. V.; Kim, Y. J.; Gholinia, A.; Haigh, S. J.; Makarovsky, O.; Eaves, L.; Ponomarenko, L. A.; Geim, A. K.; Novoselov, K. S.; Mishchenko, A. *Nat. Nanotechnol.* **2013**, *8*, 100−103.

(8) Bhandavat, R.; David, L.; Singh, G. *J. Phys. Chem. Lett.* **2012**, *3*, 1523−1530.

(9) Yang, J.; Voiry, D.; Ahn, S. J.; Kang, D.; Kim, A. Y.; Chhowalla, M.; Shin, H. S. *Angew. Chem., Int. Ed.* **2013**, *52*, 13751−13754.

(10) Matte, H. S.; Gomathi, A.; Manna, A. K.; Late, D. J.; Datta, R.; Pati, S. K.; Rao, C. N. *Angew. Chem., Int. Ed.* **2010**, *49*, 4059−4062.

(11) Zhou, K. G.; Mao, N. N.; Wang, H. X.; Peng, Y.; Zhang, H. L. *Angew. Chem., Int. Ed.* **2011**, *50*, 10839−10842.

(12) Halim, U.; Zheng, C. R.; Chen, Y.; Lin, Z.; Jiang, S.; Cheng, R.; Huang, Y.; Duan, X. *Nat. Commun.* **2013**, *4*, 2213.

(13) Cunningham, G.; Lotya, M.; Cucinotta, C. S.; Sanvito, S.; Bergin, S. D.; Menzel, R.; Shaffer, M. S. P.; Coleman, J. N. *ACS Nano* **2012**, *6*, 3468−3480.

(14) Coleman, J. N.; Lotya, M.; O'Neill, A.; Bergin, S. D.; King, P. J.; Khan, U.; Young, K.; Gaucher, A.; De, S.; Smith, R. J.; Shvets, I. V.; Arora, S. K.; Stanton, G.; Kim, H. Y.; Lee, K.; Kim, G. T.; Duesberg, G. S.; Hallam, T.; Boland, J. J.; Wang, J. J.; Donegan, J. F.; Grunlan, J. C.; Moriarty, G.; Shmeliov, A.; Nicholls, R. J.; Perkins, J. M.; Grieveson, E. M.; Theuwissen, K.; McComb, D. W.; Nellist, P. D.; Nicolosi, V. *Science* **2011**, *331*, 568−571.

(15) Smith, R. J.; King, P. J.; Lotya, M.; Wirtz, C.; Khan, U.; De, S.; O'Neill, A.; Duesberg, G. S.; Grunlan, J. C.; Moriarty, G.; Chen, J.; Wang, J.; Minett, A. I.; Nicolosi, V.; Coleman, J. N. *Adv. Mater.* **2011**, *23*, 3944−3948.

(16) Loh, K. P.; Bao, Q.; Eda, G.; Chhowalla, M. *Nat. Chem.* **2010**, *2*, 1015−1024.

(17) Li, Z.; He, M.; Xu, D.; Liu, Z. *J. Photochem. Photobiol., C: Photochem. Rev.* **2014**, *18*, 1−17.

(18) Deng, R.; Xie, X.; Vendrell, M.; Chang, Y. T.; Liu, X. *J. Am. Chem. Soc.* **2011**, *133*, 20168−20171.

(19) Yuan, Y.; Wu, S.; Shu, F.; Liu, Z. *Chem. Commun.* **2014**, *50*, 1095−1097.

(20) Zhu, C.; Zeng, Z.; Li, H.; Li, F.; Fan, C.; Zhang, H. *J. Am. Chem. Soc.* **2013**, *135*, 5998−6001.

(21) Huang, K.-J.; Wang, L.; Liu, Y.-J.; Gan, T.; Liu, Y.-M.; Wang, L.-L.; Fan, Y. *Electrochim. Acta* **2013**, *107*, 379−387.

(22) Huang, K.-J.; Liu, Y.-J.; Wang, H.-B.; Gan, T.; Liu, Y.-M.; Wang, L.-L. *Sens. Actuators, B: Chem.* **2014**, *191*, 828−836.

(23) Xi, Q.; Zhou, D.-M.; Kan, Y.-Y.; Ge, J.; Wu, Z.-K.; Yu, R.-Q.; Jiang, J.-H. *Anal. Chem.* **2014**, *86*, 1361−1365.

(24) Tonti, D.; Varsano, F.; Decker, F. *J. Phys. Chem. B* **1997**, *101*, 2485−2490.

(25) Groszek, A. J. *Nature* **1964**, *204*, 680.

(26) Lakowicz, J. *Principles of Fluorescence Spectroscopy*, 3rd ed.; Springer: New York, 2006.

(27) Zeng, L.; Yuan, Y.; Shen, P.; Wong, K.-Y.; Liu, Z. *Chem.—Eur. J.* **2013**, *19*, 8063−8067.

(28) He, S.; Song, B.; Li, D.; Zhu, C.; Qi, W.; Wen, Y.; Wang, L.; Song, S.; Fang, H.; Fan, C. *Adv. Funct. Mater.* **2010**, *20*, 453−459.

(29) Lu, C. H.; Yang, H. H.; Zhu, C. L.; Chen, X.; Chen, G. N. *Angew. Chem., Int. Ed.* **2009**, *48*, 4785−4787.

(30) Iliuk, A. B.; Hu, L.; Tao, W. A. *Anal. Chem.* **2011**, *83*, 4440−4452.

(31) Mascini, M.; Palchetti, I.; Tombelli, S. *Angew. Chem., Int. Ed.* **2012**, *51*, 1316−1332.